

## Photoelectron spectrometry of manganese vapor between 12 and 110 eV

Manfred O. Krause, Thomas A. Carlson, and Anders Fahlman\*

*Oak Ridge National Laboratory, Oak Ridge, Tennessee 37831*

(Received 4 May 1984)

The important dynamic parameters, partial photoionization cross section  $\sigma$  and angular distribution parameter  $\beta$ , have been determined for atomic Mn between 12 and 110 eV by electron spectroscopy with synchrotron radiation (ESSR). The single-electron photolines from the  $3d$  and  $4s$  subshells and the associated two-electron satellite lines were measured, and the resonance region of  $3p \rightarrow 3d$  excitation around 50 eV was studied in detail. Absolute partial cross sections were derived. For the  $3d$ -subshell properties, we find good agreement with the many-body perturbation-theory calculation (MBPT) by Garvin *et al.* over the entire energy range and with the random-phase-approximation results by Amusia *et al.* over the  $3p$  resonance region. Available calculation (MBPT) underestimates the enhancement of  $\sigma(4s)$  through the  $3p$  resonance. Where overlap exists, the experimental data by Bruhn *et al.* and by Kobrin *et al.* agree well with our results. The work on Mn, taken *in toto*, provides a good overall understanding of the photoionization dynamics of the  $3d$  transition series element Mn, which has a half-filled subshell, although a number of problems, e.g., two- and three-electron transitions and the low-energy region, remain to be further studied. A need for an accurate determination (5–10%) of the total photoabsorption cross section is indicated.

## I. INTRODUCTION

Manganese provides a convenient test case for the photoionization dynamics of a  $3d$  transition series element, because Mn has a half-filled  $3d$  subshell and otherwise filled subshells, which simplifies the theoretical treatment and the spectral features, and because Mn has a low-vaporization temperature, which simplifies the experimental procedures. It is, therefore, not surprising that several experimental and theoretical studies have been carried out recently within a short time span. Dyke *et al.*<sup>1</sup> reported the 21.2-eV photoelectron spectrum of manganese vapor; Bruhn, *et al.*<sup>2</sup> measured the  $4s$  and  $3d$  partial cross sections from 40 to 56 eV to cover the  $3p \rightarrow 3d$  resonance region; Korbin *et al.*<sup>3</sup> measured both the partial cross sections  $\sigma_i$  and the angular distribution parameter  $\beta_i$  from 50 to 72 eV emphasizing the behavior of the correlation satellites; Davis and Feldkamp<sup>4</sup> and Amusia *et al.*<sup>5</sup> calculated the  $3d$  cross section through the  $3p$  resonance in the Hartree-Slater (HS) and random-phase-approximation (RPA) models, respectively, and, finally, Garvin *et al.*<sup>6</sup> calculated  $\sigma_i$  and  $\beta_i$  for all subshells between 16 and 100 eV in both the Hartree-Fock (HF) and the many-body perturbation-theory (MBPT) models. The detailed electron emission studies were preceded by determinations of the total photoabsorption coefficient<sup>7,8</sup> of the atomic vapor between about 45 and 60 MeV.

In this work, we measured the important dynamic properties, the partial photoionization cross sections and the angular distribution parameters for single-electron emission from the  $3d$  subshell between 15 and 111 eV, from the  $4s$  subshell between 12 and 58 eV, and for two-electron transitions involving the  $3d$  and  $4s$  electrons between 30 and 58 eV. Hence, our measurements comprise and extend the ranges of the related experimental work, and provide an excellent overall test of the theoretical

models, especially the MBPT results<sup>6</sup> that span the same energy region as the experiment and are the most comprehensive to date.

Preliminary data, which we obtained during one period of synchrotron radiation beam time, have been compared with theory by Garvin *et al.*<sup>6</sup> on a relative basis. We now present the results of three time periods and, most importantly, place our data on an absolute basis by partitioning the total photoabsorption cross section into its various components of one- and two-electron processes. This is then the first time that absolute partial cross sections have been determined for a metallic vapor. However, in the absence of data for the double ionization process and the considerable uncertainty in the total photoabsorption cross section, our absolute values are much less accurate than those we reported previously for the rare gas neon.<sup>9</sup>

## II. EXPERIMENTAL

The ESSR studies (electron spectrometry with synchrotron radiation) were carried out at the Tantalus storage ring in Wisconsin with our spectrometer, which was described previously.<sup>10</sup> We use one of the electrostatic analyzers set at the magic angle  $\Theta_m$  to measure relative partial cross sections, and both analyzers placed into the directions of the major and minor axes of the polarization ellipse, either  $0^\circ$  and  $90^\circ$ , or  $90^\circ$  and  $180^\circ$  for the pair of analyzers, to measure the angular distribution parameter. These choices follow from the intensity distribution of the photoelectrons ejected from the level  $i$  at low photon energies where the dipole approximation is valid

$$I_i(\phi) \propto \frac{d\sigma_i}{d\Omega} = \frac{\sigma_i}{4\pi} \left[ 1 + \frac{\beta_i}{4} [1 + 3p \cos(2\phi)] \right]. \quad (1)$$

For a given polarization  $p$ , a so-called magic angle  $\phi = \Theta_m$  can be chosen so that  $I_i \propto \sigma_i$ . For the angles  $\phi = 0^\circ$  ( $180^\circ$ )

and  $\phi=90^\circ$ , the dipole angular distribution parameter  $\beta_i$  can be related to the corresponding measured intensities  $I(0^\circ)$  or  $I(180^\circ)$  and  $I(90^\circ)$  by

$$\beta_i = \frac{4(R-1)}{3p(R+1)-(R-1)}, \quad (2)$$

where  $R=I(0^\circ)/I(90^\circ)$  or  $I(180^\circ)/I(90^\circ)$ .

The setting  $\phi=0^\circ$  coincides with the direction of the electric field  $\vec{E}_{\parallel}$  in the source volume of our instrument and not necessarily with the (horizontal) plane of the electron orbit in the storage ring, because the electron beam position relative to the photon-optical elements and the action of the dispersive, reflective and collimating elements of the photon beam transport, including monochromator and capillary of our setup, may tilt the vector  $\vec{E}_{\parallel}$  out of the plane. For the different experimental periods and two different beam lines, we determined tilt angles of  $0^\circ$ ,  $-7.5^\circ$ , and  $-12^\circ$ . This was done by recording the full curve [Eq. (1)] from  $-90^\circ$  to  $270^\circ$  in small steps for a suitable calibrant line, such as Xe  $5p_{3/2}$  at  $h\nu=25$  eV. During a given two-week period, no significant change in the tilt angle was noticed from one beam injection to another.

The ratio  $R$  was determined in two ways: (1) by recording simultaneously the signals from one analyzer set to  $\phi=0^\circ$  and the other to  $\phi=90^\circ$  (or  $90^\circ$  and  $180^\circ$ ), and (2) by recording the signal from one analyzer only, first at  $0^\circ$  (or  $180^\circ$ ) and then at  $90^\circ$ . In the first case, effects due to fluctuations and drifts in the photon beam and vapor density are eliminated, and in the second case, differences in the response of the two analyzers are of no concern. In general, the ratios agreed quite well with each other following the needed corrections.

Possible deviations of the electron source from a homogeneous cylinder in regard to the viewing angle were checked by recording photoelectrons, for which  $\beta=0$ , as a function of angle  $\phi$ . Suitable lines with  $\beta=0\pm 0.05$  are Ar  $3p$  (16.53 eV), Ag  $4d$  (19.2 eV), Ne  $2p$  (26.7 eV), and Xe  $5p_{3/2}$  (60.3 eV). The required corrections amounted to about 10% in the ratio  $R$ .

The polarization  $p$  was measured by applying the PAX method<sup>10,11</sup> (photoelectrons for the analysis of x rays) and using He  $1s$  with  $\beta=2$  as a converter for  $h\nu>27$  eV. Below 27 eV, photolines of the other rare gases served as converters at energies where  $\beta$  values of accuracies better than  $\pm 0.1$  units have been reported.<sup>12</sup>

The relative partial cross section  $\sigma_i$  of the level  $i$  was obtained from<sup>11</sup>

$$\sigma_i = CI_i/N(h\nu)E_i(\text{kin})K_i, \quad (3)$$

where  $C$  is a factor that can be considered invariable under our experimental conditions;  $I_i$  is the photoelectron count in peak  $i$  measured at the angle  $\Theta_m$ ,  $N(h\nu)$  the number of photons of energy  $h\nu$ ;  $E_i(\text{kin})$  the kinetic energy of the photoelectron entering the analyzer, and  $K_i$  a lens factor that depends on the acceleration voltage applied to the source cell. Similarly, Eq. (3) was used to obtain the relative number of photons,  $N(h\nu)$ , by the PAX relation<sup>11</sup> in which well-known cross sections for the reference levels are utilized, such as Ne  $2p$  (Refs. 13 and 14) and Xe  $5p_{3/2}$ ,<sup>14</sup> as well as He  $1s$  (Refs. 14 and 15), Ar  $3p$  (Ref. 15), and Kr  $4p_{3/2}$ .<sup>15</sup> Then Eq. (3) becomes

$$\sigma_i = \frac{I_i E_{\text{kin}}(\text{ref}) K(\text{ref})}{I(\text{ref}) E_i(\text{kin}) K_i} \sigma(\text{ref}), \quad (4)$$

where the reference values are indicated as such, and where  $I_i$  and  $I(\text{ref})$  are normalized to the same time interval and the same electron current in the storage ring. The ratio  $K(\text{ref})/K_i$  deviates from unity only at low kinetic energies. All data were obtained with a small acceleration of either 3 or 5 V. Many results were derived from photoelectron spectra comprising all photolines. However,  $\sigma(3d)$  values were also obtained in quick succession from scans containing the  $3d$  photoline only.

The properties and settings of the monochromators used in this work are summarized in Table I. The polarization values are typical for the given energy ranges; variations of up to 3% occurred between different time periods. The energy calibration of the TGM-HEG was checked by comparing the Xe  $5p$  photolines arising from first-order radiation with the Xe  $4d$  lines and the Xe  $4d$ - $5p$  Auger lines produced by second-order radiation. In addition, the TGM-HEG settings were compared with the TGM-LEG settings between 45 and 50 eV by way of the photoelectron signal. The resulting energy calibration in the  $3p$  resonance region is accurate to about  $\pm 0.1$  eV.

Manganese of 99.99% purity was evaporated from a Ta oven heated resistively to  $900$ – $950^\circ\text{C}$  at an ambient pressure of  $(5$ – $10)\times 10^{-6}$  Pa. This was the same oven that was used earlier for Ag (Ref. 16) and later for Ga.<sup>17</sup> The vapor density in the source cell was estimated to correspond to  $(2$ – $5)\times 10^{-2}$  Pa. During operation, temperature and vapor density proved extremely stable. However, the strength of the photoelectron signal decreased steadily in time because of metal deposits in the light-carrying capillary and the vapor entrance hole of the source cell. After nine hours of operation, vapor deposits were removed from the electron source cell and the light capillary attached to the cell.

TABLE I. Properties and operating conditions of monochromators used in this work.

Monochromator	Grating lines/mm	Range (eV)	Calibration accuracy (eV)	Bandpass (Å)	Polarization
Seya	1440	12 to 25	$\leq 0.04^b$	1.6	0.96
TGM LEG <sup>a</sup>	450	18 to 50	$\leq 0.1^b$	5	0.94 to 0.88 <sup>c</sup>
TGM HEG <sup>a</sup>	1800	45 to 110	0.1 to 0.2	2	0.91 to 0.80 <sup>c</sup>

<sup>a</sup>Toroidal grating monochromator with low-energy and high-energy gratings (LEG and HEG).

<sup>b</sup>Nominal.

<sup>c</sup>Values from low-energy to high-energy limits.

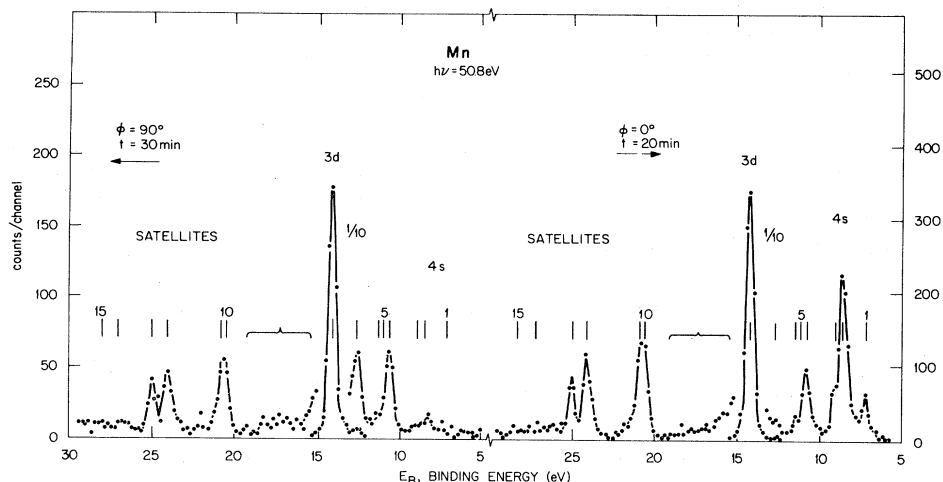


FIG. 1. Photoelectron spectrum of atomic manganese vapor as recorded in the direction of the polarization vector of the monochromatized synchrotron radiation and perpendicular to it. Lines are identified in Table II.

Spectra were recorded by scanning either the source (constant pass energy mode) or the plates of the analyzers (constant acceleration mode). Cross-section data were usually obtained in the constant acceleration mode. Signals were stored in a multichannel scaler (analyzer) which could be multiplexed. Dwell times of 200  $\mu$ s per channel were used and the energy intervals were divided into either 128 or 256 channels. Hence the time for an individual scan was short and the many scans required to obtain a spectrum with adequate statistics largely eliminated discriminatory effects from signal fluctuations and drifts. The resolution of the analyzers was  $\Delta E/E=0.01$ ; and the two analyzers had very similar characteristics.

### III. RESULTS AND DISCUSSION

#### A. The photoelectron spectrum

A full-range photoelectron spectrum of Mn is displayed in Fig. 1, showing all the photolines produced and their relative intensities in the direction of the polarization vector of the photon beam ( $\phi=0^\circ$ ) and perpendicular to the polarization vector ( $\phi=90^\circ$ ). Emission from the  $3d$  subshell is seen to be strong, and emission from the  $4s$  subshell to be weak. In addition, the angular distributions of electrons from the  $3d$  subshell, including the correlation satellites, are found to peak only slightly in the  $\phi=0^\circ$  direction ( $\beta \approx 1$ ), while those from the  $4s$  subshell, namely, peaks 1 and 2, are peaked strongly into the  $\phi=0^\circ$  direction ( $\beta \approx 2$ ).

The energies of the photoelectron peaks are given in Table II. Energies of peaks 1, 2, and 8 are taken from the tabulation of Corliss and Sugar<sup>18</sup> and served as calibrants for the other peaks, whose energies were found to be in good agreement with the values reported in Refs. 2 and 3. Peak assignments are also listed in Table II. Except for the lines 1, 2, and 8 that correspond to single-electron emission, the assignments of the other lines is not definitive. According to Corliss and Sugar, many other final

states can be assigned to the various peaks; however, we consider the given assignments to be the most likely. In the case of peaks 4 to 7,  $4s$  correlation satellites probably contribute to the  $3d^5(X)4s(Y)$  multiplet. Kobrin *et al.*<sup>3</sup> elaborate on the identification of the  $3d$  satellites, peaks 9 to 13. The peaks 14 and 15 can barely be discerned in Fig. 1, but appear clearly at an excitation energy of 55.9 eV. They are a "doublet" similar to peaks 12 and 13 and could be due to a final ionic state of the type  $3d^4 4s 5d$ .

#### B. The $3d$ subshell

The partial photoionization cross section  $\sigma_{3d}$  for the emission of a  $3d$  electron and the corresponding angular distribution parameter  $\beta_{3d}$  are displayed in Fig. 2 and in Table III over the photon-energy range covered in this ex-

TABLE II. Energies and assignments of atomic levels seen in the photo-electron spectrum of Mn in Fig. 1.

Peak	$E$ (eV)	Assignment
1	7.437 <sup>a</sup>	$3d^5(^6S)4s^7S_3$
2	8.611 <sup>a</sup>	$3d^5(^6S)4s^5S_2$
3	9.2(1)	$3d^6^5D$
4	10.9(1)	$3d^5(^4G)4s^5G$
5	11.2(1)	$3d^5(^4P)4s^5P$
6	11.6(1)	$3d^5(^4D)4s^5D$ $3d^5(^4G)4s^3G$
7	12.8(1)	$3d^5(^4F)4s^5F$
8	14.301 <sup>a</sup>	$3d^4(^5D)4s^2^3D$
9	16 to 18	$3d^4 4p; 3d^5 5s$
10	20.6(2)	$3d^4(^5D)4s 4p^5F$ $3d^5(^4D)5s$
11	21.0(2)	$3d^4(^5D)4s 4p^5P$
12	24.2(1)	$3d^4 4s 4d$
13	25.1(1)	$3d^4 4p^2$
14	27.5(2)	
15	28.5(2)	$3d^4 4s 5d$

<sup>a</sup>Reference values from Corliss and Sugar (Ref. 18).

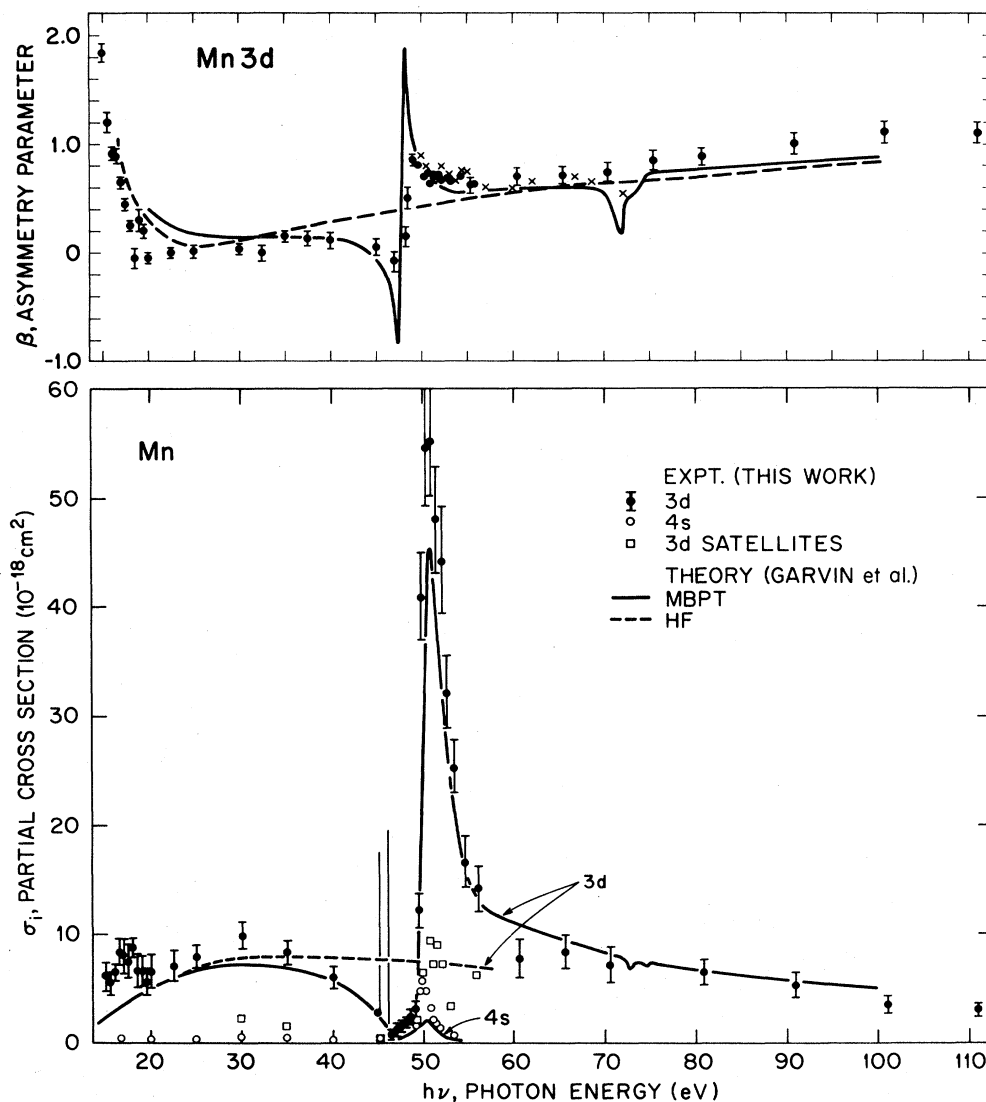


FIG. 2. Angular distribution parameter  $\beta$  of 3d photoelectrons (upper panel) and partial cross sections of 4s, 3d and satellite peaks (lower panel). Crosses ( $\times$ ) for  $\beta$  are from Ref. 3, theory from Ref. 6. The resonance near 50 eV is due to the  $3p \rightarrow 3d$  excitation into the partially filled 3d subshell of Mn.

periment. The values are averaged from the data obtained in runs during three different periods of beam time and with the aid of two different monochromators. As a result the final data differ somewhat from our first data which were presented previously by Garvin *et al.*<sup>6</sup> with their theoretical results. Also Garvin *et al.* normalized the earlier experimental data to theory at the higher energies,  $h\nu \approx 80$  eV, while the present data are normalized at  $h\nu = 45$  eV to a value of 3.5 Mb for the total photoionization cross section. The cross section at this energy was deemed to be the most reliable in the energy range of  $45 < h\nu < 60$  eV that was scanned by Bruhn *et al.*<sup>8</sup> in the absorption measurement of the Mn vapor. The results of Ref. 8 were given in absolute units on the basis of a comparison with the data<sup>19</sup> on Mn metal. The accuracy in  $\sigma_{\text{tot}}$  should not be assessed to be better than  $\pm 30\%$ . This uncertainty was not included in the errors shown in Table

III for  $\sigma_{3d}$ ; rather the errors in  $\sigma_{3d}$  reflect the uncertainty in the partition of  $\sigma_{\text{tot}}$  into its components with the aid of the photoelectron line intensities at  $h\nu = 45$  eV. It should be noted that, in the absence of any determinations, the cross section for double photoionization was not considered in the partition process. Hence  $\sigma_{3d}$ , as well as the other partial cross sections, could decrease by approximately 10%.

The theoretical cross section  $\sigma_{3d}$  by Garvin *et al.*<sup>6</sup> is in good agreement with the observation over almost the entire range. Even if we allowed for the maximum estimated error of 35%, theory would still well reproduce the shape of the curve. The difference between theory and experiment in the  $3p \rightarrow 3d$  resonance peak ( $h\nu \approx 50$  eV) is well within the error arising from the uncertainty in  $\sigma_{\text{tot}}$ . However, a definite discrepancy occurs below  $h\nu \approx 20$  eV. There, resonances due to the excitation of a 3d electron

TABLE III. Partial photoionization cross section and angular distribution parameter for  $3d$  electrons of atomic manganese.

$h\nu$ (eV)	$\sigma_{3d}(10^{-18} \text{ cm}^2)$	$\beta_{3d}$	$h\nu$ (eV)	$\sigma_{3d}(10^{-18} \text{ cm}^2)$	$\beta_{3d}$
15.0	6.1(1.3)	1.84(8)	48.3	2.3(5)	0.15(8)
15.5	5.4(1.2)	1.20(9)	48.7	3.1(7)	0.5(1)
16.0	6.4(0.8)	0.91(6)	49.3	12.1(1.5)	0.85(5)
16.5	8.3(1.5)	0.89(7)	49.8	40.9(4.5)	0.80(6)
17.0	8.0(1.7)	0.64(6)	50.3	54.6(5.4)	0.70(6)
17.5	7.4(1.6)	0.44(5)	50.8	55.2(5.4)	0.71(7)
18.0	8.7(0.9)	0.25(5)	51.1		0.65(7)
18.5	6.6(1.6)	-0.05(9)	51.3	48.0(5.2)	0.72(5)
19.0	6.6(1.5)	0.3(1)	51.8	44.1(5.1)	0.72(5)
19.5	5.5(1.3)	0.20(6)	52.3	32.0(3.4)	0.66(6)
20.0	6.6(1.6)	-0.05(5)	52.8		0.68(6)
22.5	7.0(1.5)	0.00(4)	53.3	25.4(2.7)	0.65(8)
25.0	7.8(1.2)	0.02(4)	54.4	16.5(2.4)	0.70(9)
30.0	9.8(1.4)	0.03(5)	55.8	14.1(2.2)	0.61(6)
32.5		0.00(7)	60.4	7.7(1.9)	0.70(8)
35.0	8.2(1.2)	0.15(6)	65.5	8.3(1.6)	0.71(8)
37.5		0.13(7)	70.6	7.2(1.9)	0.75(8)
40.0	5.9(1.2)	0.12(7)	75.6		0.85(9)
45.0	2.73 <sup>a</sup>	0.06(8)	80.7	6.6(1.3)	0.88(9)
46.5	0.8(0.4)		90.8	5.5(1.2)	1.0(1)
47.1	1.2(7)	-0.08(9)	101	3.6(0.8)	1.0(1)
47.8	1.5(4)		111	3.0(0.7)	1.1(1)

<sup>a</sup>Reference value based on  $\sigma$  (total) = 3.5 Mb (Ref. 8) and our partition of  $\sigma$  (total) at  $h\nu = 45.0$  eV.

and two-electron excitations are expected to take place, and these processes were not taken into account in the MBPT nor any other calculation.<sup>6</sup>

The experimental values of the angular distribution parameter  $\beta_{3d}$  display an equally satisfactory agreement with the theoretical values calculated by Garvin *et al.*<sup>6</sup> as do the  $\sigma_{3d}$  data. Since the  $\beta$  values are based on ratios of (differential) cross sections, no normalization is needed and no errors due to this source can be introduced. Thus the agreement is especially gratifying. We note, however, that the experimental  $\beta$  values are greater by 0.1 to 0.2 units than the prediction at the higher photon energies. As for  $\sigma_{3d}$ , the experimental and theoretical  $\beta_{3d}$  values differ somewhat below 20 eV due to excitation processes not included in the theory. The steep rise toward  $\beta = 2$  at the very low photon energies is in accord with the Hartree-Fock results.<sup>6</sup> The only other available experimental data, those of Kobrin *et al.*<sup>3</sup> between 50 and 72 eV, agree well with our determinations.

As seen in Fig. 2, both the  $\sigma_{3d}$  and the  $\beta_{3d}$  curves are dominated by the resonance near 50 eV that arises from the coupling of the  $3p \rightarrow 3d$  excitation channel with the  $3d \rightarrow \epsilon f; \epsilon p$  ionization channels. Other channels couple as well, but as the calculations and the good agreement between theory and experiment demonstrate, the  $3p \rightarrow 3d$  and  $3d \rightarrow \epsilon f; \epsilon p$  channels are, indeed, the major pathways near  $h\nu = 50$  eV. If the channel coupling is not taken into account, as in the single-particle HF calculation<sup>6</sup> plotted in Fig. 2, then no excursions occur in  $\sigma_{3d}$  and  $\beta_{3d}$  around the  $3p \rightarrow 3d$  resonance. Outside the resonance we observe a satisfactory account of the experimental findings by the HF model indicating at most a weak coupling between the

$3d \rightarrow \epsilon f; \epsilon p$  and the  $4s \rightarrow \epsilon p$  continuum channels and, at the higher energies, between the  $3d \rightarrow \epsilon f; \epsilon p$  and  $3p \rightarrow \epsilon d; \epsilon s$  continuum channels.

The resonance region has now been investigated in five experimental<sup>2,3,7,8</sup> and three theoretical<sup>4-6</sup> studies. In Fig. 3 and Table IV, we compare the various results on the  $3d$  partial cross section. The data of Refs. 2 and 3 are normalized at 50 eV to our absolute values. We note a satisfactory agreement between the three sets of experimental data in regard to (a) the width of the resonance, (b) the position of the resonance, and (c) the drop off toward higher photon energies as characterized by  $I_p/I_{60}$ , which is the intensity at the peak maximum relative to that at  $h\nu = 60$  eV. However, our  $I_p/I_{45}$  ratio which describes the low-energy side of the resonance is more pronounced than the ratio measured by Bruhn *et al.*<sup>2</sup> The theoretical curves by Garvin *et al.*<sup>6</sup> and by Amusia *et al.*<sup>5</sup> agree quite well with the observation, while the earlier calculation by Davis and Feldkamp<sup>4</sup> yield a resonance that is too broad. Numerical values of criteria suitable for describing the resonance are summarized in Table IV and show the many-body perturbation-theory (MBPT) model used by Ref. 6 in two slightly different approaches of the coupling procedure<sup>6</sup> and the random-phase-approximation (RPA) model used in Ref. 5 to represent the essential features of the resonance.

The theoretical results of the behavior of  $\beta_{3d}$  over the resonance itself is not quite as good as for  $\sigma_{3d}$ . The excursions of  $\beta_{3d}$  are predicted to be much sharper than observed by us (Fig. 2). Even if the finite bandpass, about 0.4 eV, is removed, the experimental spikes will still remain below theory by about 0.4 units in  $\beta$ .

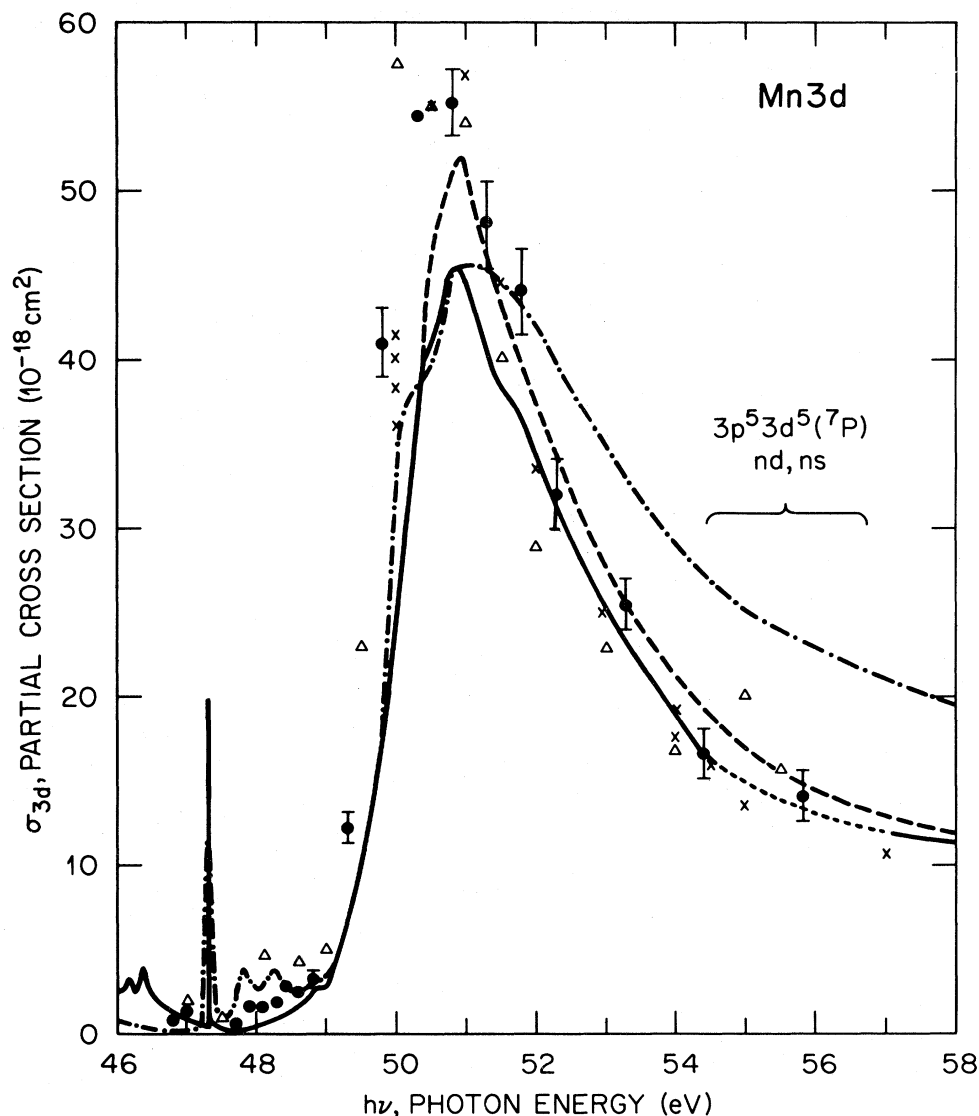


FIG. 3. Comparison of our results (●) for the  $3d$  subshell (peak 8 of Fig. 1) with other experimental data and theoretical results. Experiment: Bruhn *et al.*, Ref. 2 ( $\Delta$ ); Kobrin *et al.*, Ref. 3 ( $\times$ ); theory: Davis and Feldkamp, Ref. 4 (dash-dot), Garvin *et al.*, Ref. 6 (solid and dash lines, as obtained by MBPT using the interacting resonance method and the coupled equation method, respectively). The RPA calculation of Amusia *et al.*, Ref. 5, virtually coincides with the dash curve. Our data are referred to the total absolute cross section at 45 eV, and data of Refs. 2 and 3 are normalized to ours at 50.5 eV.

In Fig. 3 we omitted the resonance spikes predicted by Garvin *et al.*<sup>6</sup> to occur between 55 and 57 eV. Delineation of these resonances, even if they should be much broader than predicted, would require a narrower bandpass than available in this experiment. A similar statement can be made concerning resonances between 45 and 48 eV.<sup>4,6</sup>

The  $3d$  partial cross section dominates the  $3p \rightarrow 3d$  resonance, as seen from Fig. 2. As a consequence, the total absorption cross section should be nearly identical with the  $3d$  partial cross section. However,  $\sigma_{\text{tot}}$  does not exhibit the high contrast shown by  $\sigma_{3d}$  and the resonance appears to be much broader in absorption<sup>7,8</sup> than in emission. The discrepancy as indicated in Table IV for the data of Ref. 8 should probably be ascribed to the limited

TABLE IV. Relative peak height and width of  $3d$  resonance in manganese. Peak heights are referred to values at 45 and 60 eV, and width is given at  $\frac{2}{3}$  of maximum.

Source	$I_p/I_{45}$	$I_p/I_{60}$	$W$ (eV)
This work, expt.	20(3)	5.2(4)	2.1
Bruhn, Ref. 2, expt.	13	4.7 <sup>a</sup>	2.0
Kobrin, Ref. 3, expt.		5.9	1.9
Amusia, Ref. 5, theor.	18	5.1	2.0
Davis, Ref. 4, theor.	33	2.4	3.8
Garvin, Ref. 6, theor. 1	17	4.2	2.3
Garvin, Ref. 6, theor. 2	18	5.1	1.8
Bruhn, Ref. 8, abs. <sup>b</sup>	3.7	1.7	3.0

<sup>a</sup>Extrapolated value.

<sup>b</sup>Total absorption coefficients, expt.

TABLE V. Relative intensities,  $I$ , of spectral lines (1–15) of Fig. 1. Values are normalized to  $I(3d)=100$  and refer to the magic angle of observation.

$h\nu$ (eV)	4s and 4s satellites			3d satellites			
	$^7S(1)$	$^5S(2)$	(3 to 7)	(9)	(10/11)	(12/13)	(9–15)
16.0	3.5(4)	1.7(4)					
20.0	2.8(4)	1.4(3)					
25.0	2.4(4)	1.6(3)	4.4(7)				
30.0	2.7(5)	2.5(3)	4.1(8)				22(8)
35.0	2.4(4)	2.2(3)	4.0(6)	3.9(1.1)	7.7(1.2)	5.5(1.5)	17(4)
40.0	2.5(6)	2.1(5)					
45.2	7(2)	7(2)	6(2)				14(6)
48.3	12(2)	54(4)	50(8)	35(7)	20(6)	25(8)	80(18)
49.3		38(6)					
49.8	2.2(2)	12(1)	8(1)	2.5(5)	6.5(9)	6.7(9)	17(3)
50.3	1.5(3)	7(1)	5(1)				
50.7	1.0(3)	5.2(8)	6(1)	4.6(8)	5.3(7)	6.7(8)	18(3)
51.1	0.7(2)	3.5(5)	5(1)	0.6(2)	6.5(9)	7(1)	15(2)
51.4		4.0(6)	3.5(7)	0.9(3)	7.6(1.2)	7.7(1.2)	19(2)
51.8	0.7(3)	2.3(6)	2.4(6)	0.8(3)	6.9(1.2)	7.2(1.4)	16(2)
53.3		2.4(6)	2(1)	1.6(5)	5.5(1.1)	5.1(1.2)	14(2)
55.8		1.1(4)	4(2)	4.8(9)	9.6(2.1)	15(3)	45(8)

dynamic range of photographic recording used in the absorption measurements. It is this suspected deficiency that caused us to normalize our data to  $\sigma_{\text{tot}}$  below the resonance at 45 eV rather than at the top, where the signals would be much stronger.

### C. The 4s subshell

Emission from the 4s subshell leads to a multiplet in the photoelectron spectrum. The strong  $^7S_3$  and  $^5S_2$  components can be identified unambiguously, while other term components<sup>18</sup> whose intensity could reside in peaks 4–7 coincide with correlation satellites of which peak 3 is a clearcut example. In certain instances, angular distribu-

tion studies can aid in resolving such overlapping lines of different origin, but in this case, no definite identifications can be made on the basis of  $\beta$  because, as Manson and Starace<sup>20</sup> have shown for  $\beta_s$  of atoms with open  $p$  subshells,  $\beta_{4s}$  of Mn may assume different, nonspecific values for the different terms. The small intensity of the satellite line 3 compared to the 4s lines 1 and 2 suggest, however, that the satellite contributions to peaks 4–7, which require a higher excitation energy than peak 3, are not dominant.

We consider now the 4s lines 1 and 2,  $3d^5(^6S)4s^7,^5S$ . Their relative intensities are tabulated in Table V and their absolute partial cross sections plotted in Fig. 2. An expanded view of  $\sigma_{4s}$  is given in Fig. 4 over the  $3p \rightarrow 3d$

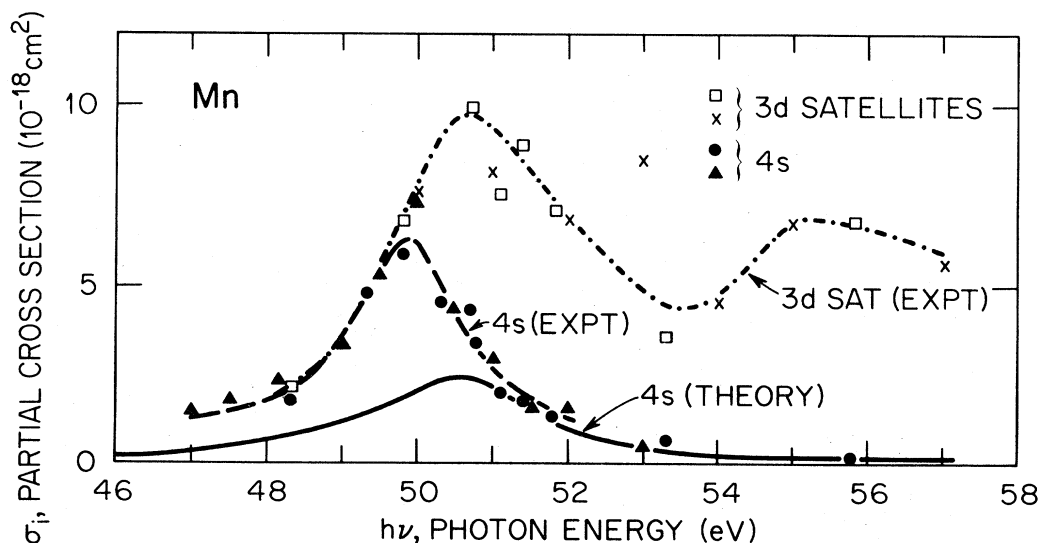


FIG. 4. Expanded view of the behavior of 4s ( $^7,^5S$ ) and satellite partial cross sections in the  $3p \rightarrow 3d$  resonance regime. Our values ( $\bullet$ ) and Bruhn *et al.*, Ref. 2 ( $\blacktriangle$ ), for 4s; our values ( $\square$ ) and Kobrin *et al.*, Ref. 3 ( $\times$ ), for the satellites. The MBPT results are from Garvin *et al.*, Ref. 6. Experimental values are referred to  $\sigma_{3d}$ , which is normalized to  $\sigma_{\text{tot}}$  at 45 eV.

TABLE VI. Angular distribution parameter  $\beta$  for the weaker  $4s$  lines and  $3d$  satellites (numbers refer to labels of Fig. 1).

$h\nu$ (eV)	4s satellites			3d satellites			
	(4 to 6)	(7)	(4 to 7)	(9)	(10/11)	(12/13)	(14/15)
49.2			0.3(2)	0.2(2)	1.0(2)	0.7(2)	
49.7			0.35(10)	0.4(2)	1.2(2)	1.0(2)	
50.3	0.5(1)	-0.4(2)	0.35(10)	0.6(2)	1.3(2)	1.0(2)	0.7(4)
50.8			0.6(2)	0.4(3)	1.0(2)	0.6(2)	1.4(4)
51.3	0.2(2)	-0.3(2)	0.2(2)	0.6(3)	1.0(2)	0.6(2)	
51.8	0.6(2)	-0.2(2)		1.1(3)	1.0(2)	0.8(3)	
52.3			0.0(3)	0.5(3)	0.8(3)	0.7(3)	
53.3			-0.2(3)	0.1(2)	1.1(3)	1.2(4)	0.6(4)
54.4					1.0(3)	0.3(3)	
55.4				-0.1(3)	0.8(3)	0.2(3)	
55.8				0.0(3)	0.9(3)	0.4(3)	0.2(3)

resonance region. As for  $\sigma_{3d}$ , an enhancement in  $\sigma_{4s}$  occurs due to the coupling of the  $4s \rightarrow \epsilon p$  channel with the  $3p \rightarrow 3d$  excitation channel and  $3d \rightarrow \epsilon f; \epsilon p$ . Coupling of these, and other, channels was considered by Garvin *et al.*<sup>6</sup> and their results are compared in Fig. 4 with the experimental results which include the determinations by Bruhn *et al.*<sup>2,21</sup> A slight shift in position and a considerable underestimate of the resonance enhancement by theory is noted, and the underestimate would be accentuated if part or all of the intensity residing in peaks 4–7 were to be included in the experimental curve. The disagreement for the  $s$  subshell is reminiscent of the behavior of  $\sigma_{5s}$  of Xe in the delayed  $4d$  maximum. There, the theory that gives excellent results for the other subshells fails to correctly predict the  $s$  cross section. However, in the case of Xe, the random-phase approximation (RPA) calculation overestimates  $\sigma_{5s}$  within the delayed maximum.<sup>14</sup>

No systematic study of  $\beta$  was carried out over the entire energy range for the lines associated with the  $4s$  subshell. In the resonance region between 49 and 51.8 eV, the  $\beta$  values for lines 1 and 2 were found to be close to 2, those for lines 4–6 to be about 0.5 and those for line 7 to be consistently negative (Table VI). Preliminary data in the region of the  $3d$  threshold, especially over the Rydberg series between 12 and 14 eV, show strong variations of the  $\beta$  parameters for the  $^7S$  and  $^5S$  lines. These variations are also reflected in the branching ratio  $^7S/^5S$  as

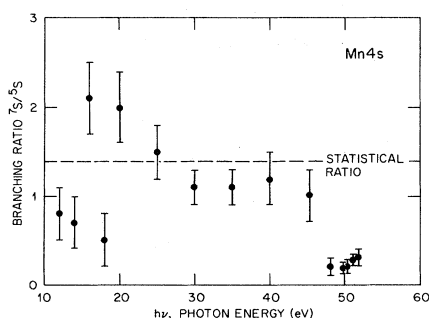


FIG. 5. Branching ratio for the main  $4s$  lines of Mn. Note the low ratio within the  $3p \rightarrow 3d$  resonance. The excursions at  $h\nu < 20$  eV will require scrutiny with a finer energy mesh.

seen in Fig. 5. Over the  $3p \rightarrow 3d$  resonance the branching ratio has a very low value of about 0.2 which is mainly due to an enhancement of the cross section for the  $^5S$  component (compare Table V). In the region outside excitation resonances,  $25 < h\nu < 40$  eV, the branching ratio is close to but somewhat lower than the statistical ratio.

#### D. The correlation satellites

The photoelectron spectrum of Fig. 1 shows many lines that must be associated with two-electron transitions which lead to the final states suggested in Table II. Kobrin *et al.*<sup>3</sup> have made a detailed study of the most likely final ionic states and the satellite intensities at photon energies above 50 eV. We measured the satellite intensities at energies ranging from 30 to 56 eV and the  $\beta$  parameters over the  $3p$  resonance region. Relative intensities are given in Table V, and the  $\beta$  parameters are presented in Table VI. As pointed out in the preceding section, the assignment of  $4s$  satellites to lines 4–7 is not unique, but the lines 10–15 can be definitely associated with two-electron processes involving the  $3d$  subshell. This follows on energy arguments,<sup>18</sup> and the similarity of the  $\beta$  parameter for peaks 10–13 and, to a lesser degree, for peaks 14 and 15 suggests that a  $3d$  electron is ionized concomitant with the excitation of a  $4s$  electron. The lower  $\beta$  values for the peak structure 9 could indicate an admixture from the  $4s$  satellite structure.

The partial cross section for the  $3d$  satellites is plotted in Fig. 2 and, on a larger scale, in Fig. 4. As the other ionization channels, these channels of two-electron transitions also gain strength in the  $3p \rightarrow 3d$  excitation regime. A secondary rise in the cross section is observed around 56 eV in the region where Garvin *et al.*<sup>6</sup> predict resonances due to higher excitation states of the type  $3p \rightarrow \epsilon s; ns$  and  $3p \rightarrow \epsilon d; nd$ . We find the satellite intensities reported by Kobrin *et al.*<sup>3</sup> to be in satisfactory agreement with our determination.

#### IV. CONCLUDING REMARKS

In this comprehensive ESSR study of atomic manganese vapor, both the intensities and the photoelectron angular distributions were measured for one- and two-

electron processes involving the  $4s$  and  $3d$  subshells. The measurements extended up to 110 eV and included the important  $3p \rightarrow 3d$  resonance around 50 eV. Our results are in good agreement with the data of two other groups each of which have studied several aspects of the problem over the resonance region. We have placed our intensity measurements on an absolute scale and have found the resulting absolute partial cross section of the  $3d$  subshell to be in good accord with the many-body calculations, especially the MBPT of Garvin *et al.*,<sup>6</sup> who have included the salient ionization and excitation channels. The effect of the resonance on the  $4s$  ionization channel is, however, underestimated by theory.

This work emphasizes the need for more determinations, and more accurate determinations, of total photoabsorption cross sections for metal vapors than are now available. This would allow a comparison of experiment and theory not only on a relative basis but on the more rigorous absolute scale for other atoms as well.

Although this and related studies elsewhere showed that it is now possible to obtain consistent results on an atomic vapor and that the experimental data are in satisfactory agreement with many-body theoretical calculations, a number of problems remain. There are especially problems concerning the final identification and dynamic behavior of the correlation satellites and the many-channel interactions at low energies near the  $3d$  ionization threshold.

#### ACKNOWLEDGMENTS

This research was sponsored by the Division of Chemical Sciences, Office of Basic Energy Sciences, U.S. Department of Energy under Contract No. DE-AC05-84OR21400 with the Martin Marietta Energy Systems, Inc. The Synchrotron Radiation Center at Stoughton, Wisconsin is operated under National Science Foundation Grant No. DMR-80-20164.

\*Permanent address: Department of Physics and Measurement Technology, Linköping Institute of Technology, S-581 83 Linköping, Sweden.

<sup>1</sup>J. M. Dyke, N. K. Fayad, A. Morris, and I. R. Trickle, *J. Phys. B* **12**, 2985 (1979).

<sup>2</sup>R. Bruhn, E. Schmidt, H. Schröder, and B. Sonntag, *Phys. Lett.* **90A**, 41 (1982).

<sup>3</sup>P. H. Kobrin, U. Becker, C. M. Truesdale, D. W. Lindle, H. G. Kerkhoff, and D. A. Shirley (unpublished).

<sup>4</sup>L. C. Davis and L. A. Feldkamp, *Phys. Rev. A* **17**, 2012 (1978); *Phys. Rev. B* **23**, 6239 (1981).

<sup>5</sup>M. Ya. Amusia, V. K. Ivanov, and L. V. Chernysheva, *J. Phys. B* **14**, L19 (1981).

<sup>6</sup>L. J. Garvin, E. R. Brown, S. L. Carter, and H. P. Kelly, *J. Phys. B* **16**, L269 (1983).

<sup>7</sup>J. P. Connerade, M. W. D. Mansfield, and M. A. P. Martin, *Proc. Soc. London, Ser. A* **350**, 405 (1976).

<sup>8</sup>R. Bruhn, B. Sonntag, and H. W. Wolff, *Phys. Lett.* **69A**, 9 (1978).

<sup>9</sup>F. Wuilleumier and M. O. Krause, *Phys. Rev. A* **10**, 242 (1974).

<sup>10</sup>M. O. Krause, T. A. Carlson, P. R. Woodruff, *Phys. Rev. A* **24**, 1374 (1981).

<sup>11</sup>M. O. Krause, in *Atomic Inner-Shell Processes*, edited by B.

Crasemann (Academic, New York, 1975), Vol. II, pp. 33–81.

<sup>12</sup>See, e.g., J. Kreile and A. Schweig, *J. Electron Spectrosc. Relat. Phenom.* **20**, 191 (1980); D. M. P. Holland, A. C. Parr, D. L. Ederer, J. L. Dehmer, and J. B. West, *Nucl. Instrum. Methods* **195**, 331 (1982).

<sup>13</sup>F. Wuilleumier and M. O. Krause, *J. Electron Spectrosc. Relat. Phenom.* **15**, 15 (1979).

<sup>14</sup>M. O. Krause, in *Synchrotron Radiation Research*, edited by H. Winick and S. Doniach (Plenum, New York, 1980), pp. 101–156.

<sup>15</sup>G. V. Marr and J. B. West, *At. Data Nucl. Data Tables* **18**, 497 (1976).

<sup>16</sup>M. O. Krause, P. R. Woodruff, and T. A. Carlson, *J. Phys. B* **14**, L673 (1981).

<sup>17</sup>M. O. Krause, F. Cerrina, and A. F. Fahlman, *Phys. Rev. Lett.* **50**, 1118 (1983).

<sup>18</sup>C. Corliss and J. Sugar, *J. Phys. Chem. Ref. Data* **6**, 1253 (1977).

<sup>19</sup>B. Sonntag, R. Haensel, and C. Kunz, *Solid State Commun.* **7**, 597 (1969).

<sup>20</sup>S. T. Manson and A. F. Starace, *Rev. Mod. Phys.* **54**, 389 (1982).

<sup>21</sup>Absolute values for the data of Ref. 2 were obtained by reference to  $\sigma_{3d}$  which was normalized to our data at 50.5 eV.